

CHEMISTRY & SUSTAINABILITY

# CHEM **SUS** CHEM

ENERGY & MATERIALS

## Accepted Article

**Title:** Efficient and Highly Selective Solvent-Free Oxidation of Primary Alcohols to Aldehydes Using Bucky Nanodiamond

**Authors:** Yangming Lin, Kuang-Hsu (Tim) Wu, Linhui Yu, Saskia Heumann, and Dangsheng Su

This manuscript has been accepted after peer review and appears as an Accepted Article online prior to editing, proofing, and formal publication of the final Version of Record (VoR). This work is currently citable by using the Digital Object Identifier (DOI) given below. The VoR will be published online in Early View as soon as possible and may be different to this Accepted Article as a result of editing. Readers should obtain the VoR from the journal website shown below when it is published to ensure accuracy of information. The authors are responsible for the content of this Accepted Article.

**To be cited as:** *ChemSusChem* 10.1002/cssc.201700968

**Link to VoR:** <http://dx.doi.org/10.1002/cssc.201700968>

WILEY-VCH

[www.chemsuschem.org](http://www.chemsuschem.org)

A Journal of



# Efficient and Highly Selective Solvent-Free Oxidation of Primary Alcohols to Aldehydes Using Bucky Nanodiamond

Yangming Lin,<sup>[a,b,c]</sup> Kuang-Hsu (Tim) Wu,<sup>[a]</sup> Linhui Yu,<sup>[d]</sup> Saskia Heumann,<sup>[c]</sup> and Dang Sheng Su\*<sup>[a,e]</sup>

Dedication ((optional))

**Abstract:** Selective oxidation of alcohols to aldehydes is widely applicable to the synthesis of various green chemicals. The poor chemo-selectivity for complicated primary aldehydes over state-of-the-art metal-free or metal-based catalysts represents a major obstacle for industrial application. Here we report on bucky nanodiamond as a potential green catalyst which exhibits excellent chemo-selectivity and cycle stability in the selective oxidation of primary alcohols in diverse structures (22 examples, including aromatic, substituted aromatic, unsaturated, heterocycle and linear chain alcohols) to their corresponding aldehydes; the results are even comparable to the reported transition metal catalysts and conventional Pt/C and Ru/C catalysts for certain substrates under solvent-free conditions. The possible activation process of surface oxygen groups and defect species to oxidant and substrate are revealed with model catalysts, ex-situ electrochemical measurement and ex-situ attenuated total reflectance. The zigzag edges of  $sp^2$  carbon planes have been shown to play a key role in these reactions.

## Introduction

Selective oxidation of alcohol to aldehyde is a key reaction in organic synthesis and will likely play a significant role in the development of value-added chemicals.<sup>1-4</sup> Metal-based, especially noble-metal materials, have been considered to be the most important catalysts for heterogeneous alcohol oxidation,<sup>5-8</sup> but the toxicity, unsustainability and the complex preparation process of catalysts or the low chemo-selectivity for

desired aldehydes further hinders their industrial application.<sup>9-15</sup> Over the past few years, nanocarbon catalysis are recognized as promising candidates to meet the requirement of sustainable and green chemistry.<sup>16-19</sup> Some achievements have shown the positive effects of nanocarbon materials for the oxidation reaction of simple aromatic alcohols (e.g. benzyl alcohol, substituted benzyl alcohol) by using various organic reagents as solvents and in the presence of particular oxidants, such as nitric acid, t-butylhydroperoxide (TBHP),  $H_2O_2$  and  $O_2$ ,<sup>20-26</sup> but there are few studies on the feasibility of carbon materials for the complicated alcohols (e.g., unsaturated, heterocycle and linear chain alcohols). Moreover, most of recent research objectives still focuses on the catalytic performance of newly developed catalysts for simple aromatic alcohols rather than on understanding the activation process of reactants or oxidants by the used catalysts. In this case, only a few studies could provide convincing evidence for the activation of the oxidant (e.g., TBHP and substrates over carbon materials (e.g., surface active sites). The roles of surface different oxygen groups and defects in the reactions have rarely been reported, and the interaction at interface between catalyst and oxidant or substrate remains elusive and controversial. It is therefore highly important to clarify the active sites and the corresponding activation process into more detail as an effort to elucidate their underlying catalytic activity for other complicated substrates.

Bucky nanodiamond (BND), a class of  $sp^2/sp^3$  hybrid material, consists of a  $sp^3$  carbon core covered by a few  $sp^2$  graphite-like layers that can be prepared by graphitizing purified nanodiamond (ND) at different temperatures under an inert atmosphere or in vacuum (Scheme 1,  $T < 1500$  °C). Such hybrid structure has both remarkable properties of surface graphitic nanomaterials and intrinsic nature of a diamond core.<sup>27</sup> In the previous studies, BND has been shown to be a promising catalyst in gas-phase reactions due to its unique structure and electronic properties.<sup>28-29</sup> Here, we demonstrate the excellent catalytic activity of BND for selective oxidation of complicated alcohols (22 examples) to their corresponding aldehydes. To the best of our knowledge, this is the first time that the alcohols in a range of diverse structures can be catalyzed only by nanocarbons with decent activity, even under the solvent-free condition. Through comparative experiments with model catalysts, ex-situ electrochemical measurement and ex-situ attenuated total reflectance, we are able to show the possible activation process of the oxidant (TBHP) and substrate (benzyl alcohol as probe) by the surface oxygen groups and the defects, with a proposition of possible catalytic mechanism.

[a] Dr. Y.M. Lin, Dr. K.-H. (Tim) Wu, Prof. Dr. D.S. Su  
Institute of Metal Research, Chinese Academy of Sciences  
72 Wenhua Road, Shenyang, 110016, P.R.China  
E-mail: dssu@imr.ac.cn

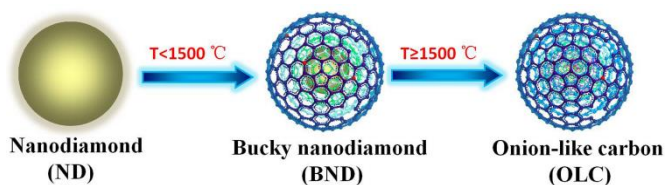
[b] Dr. Y.M. Lin  
School of Chemistry and Materials Science, University of Science  
and Technology of China, Hefei, 230001, P. R. China

[c] Dr. Y.M. Lin, Dr. S. Buller  
Max Planck Institute for Chemical Energy Conversion,  
Stiftstrasse 34–36, Mülheim an der Ruhr, 45470, Germany

[d] Dr. L. Yu  
Research Institute of Photocatalysis, Fuzhou University,  
Fuzhou 350002, P. R. China

[e] Prof. Dr. D.S. Su  
Department of Inorganic Chemistry, Fritz Haber Institute of the Max  
Planck Society, Faradayweg 4-6, Berlin, 14195, Germany

Supporting information for this article is given via a link at the end of the document. ((Please delete this text if not appropriate))



**Scheme 1.** The phase transformation of ND to BND and onion-like carbon (OLC). The surface of BND and OLC should be rather irregular  $sp^2$  carbon fragments, although multiple perfect graphitic shells were displayed for simplicity.

## Results and Discussion

The HRTEM images of ND, BND and onion-like carbon (OLC) are shown in Figure S1. The surface of purified ND is covered by amorphous and disordered carbon. The identified interlayer spacing of 0.340 nm in the outer shell and the lattice spacing of 0.206 nm in the core can be assigned to the (002) plane of graphite and (111) plane of diamond, respectively.<sup>30-31</sup> Depending on the calcination temperature, the number of graphite-like shells of BND increases from two layers of 900BND to several layers of 1300BND. When the temperature is further increased to above 1500 °C (Scheme 1), BND could completely transform into OLC that has multiple layers of curved  $sp^2$  carbon concentric shells. The particle sizes of all ND, BND and OLC samples are about 5-8 nm.

**Table 1.** Selective oxidation of benzyl alcohol by various samples under different conditions.<sup>[a]</sup>

Entry	Catalyst	$S_{\text{BET}}$ ( $\text{m}^2$ $\text{g}^{-1}$ )	Solvent	Con. (%)	Sel. (%)	Decomposition efficiency (%) of TBHP
1	---	---	TFT	2.5	90.3	1.8
2	ND	313	TFT	4.5	98.2	14.9
3	900BND	342	TFT	7.0	>99	28.5
4	1100BND	350	TFT	8.1	>99	38.7
5	1300BND	386	TFT	13.6	>99	69.5
6	1500OLC	463	TFT	11.4	98.3	56.8
7	1600OLC	476	TFT	9.3	95.9	43.2
8	Graphene	492	TFT	7.8	96.8	34.6
9	Graphite oxide	201	TFT	4.9	97.3	24.9
10 <sup>[b]</sup>	1300BND	386	TFT	62.3	97.1	>99
11	1300BND	386	---	13.4	>99	68.8
12	5 wt% Pt/C (Alfa)	---	---	16.3	85.2	>99
13 <sup>[c]</sup>	5 wt% Pt/C (Wako)	---	ethanol	9	87	---
14	5 wt% Ru/C (Alfa)	---	---	13.7	81.3	>99
15 <sup>[d]</sup>	5 wt% Ru/C (Wako)	---	ethanol	22	60	---
16 <sup>[e]</sup>	Au-Pt/AC	---	---	~21	~50	---
17 <sup>[e]</sup>	Pd-Pt/AC	---	---	~17	~45	---
18 <sup>[f]</sup>	Au/TiO <sub>2</sub>	3.5	---	63	79	---
19 <sup>[g]</sup>	Au/U <sub>3</sub> O <sub>8</sub>	7	---	100	85	---

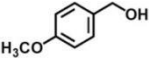
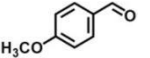
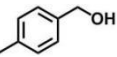
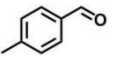
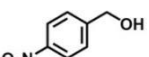
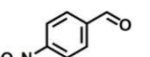
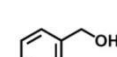
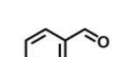
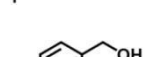
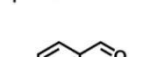
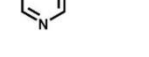
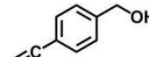
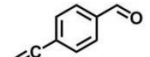
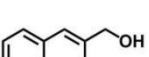
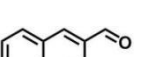
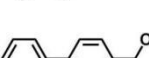
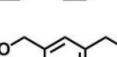
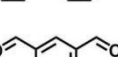
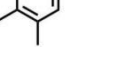
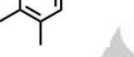
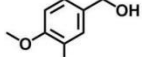
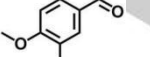
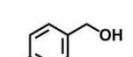
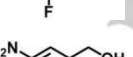
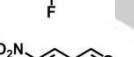
20 <sup>[h]</sup>	0.1% Fe/ 1300BND	386	TFT	13.9	>99	74.5
21 <sup>[i]</sup>	0.1% Cr/ 1300BND	386	TFT	12.5	>99	71.8

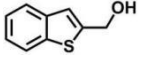
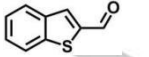
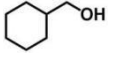
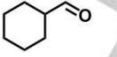
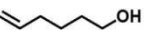
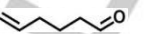
[a] Reaction condition: 10 mg catalyst, 2.0 mmol substrate, 2 mmol 65 wt% tert-butyl hydroperoxide (TBHP), 5 mL trifluorotoluene (TFT), 70 °C, 4 h. [b] 24 h. [c] Ref. 26, 1.1 mmol substrate, 100 mg catalyst, 120 °C, 3 h, O<sub>2</sub> as terminal oxidant. [d] Ref. 26, 1.1 mmol substrate, 20 mg catalyst, 120 °C, 3 h, O<sub>2</sub> as terminal oxidant. [e] Ref. 32, 47 mmol substrate, 47 mmol TBHP, metal/substrate=6500, 80 °C, 24 h. [f] Ref. 33, 52 mmol substrate, 78 mmol TBHP, 500 mg catalyst, 94 °C, 2 h. [g] Ref. 34, 52 mmol substrate, 78 mmol TBHP, 500 mg catalyst, 94 °C, 0.5 h. [h] Fe(NO<sub>3</sub>)<sub>3</sub> as precursor, annealed at 573K for 1h. [i] Cr(NO<sub>3</sub>)<sub>3</sub>·9H<sub>2</sub>O as precursor, annealed at 573K for 1h. Desired product: benzaldehyde.

Table 1 is a summary of the selective oxidation of benzyl alcohol to benzaldehyde over various carbon materials under different conditions. Without catalysts, only 2.5% benzyl alcohol could be converted. The corresponding selectivity towards benzaldehyde is 90.3% (Table 1, entry 1) in the presence of TBHP. Among the three BND samples treated at different temperatures (entries 3-5), 1300BND (treated at 1300 °C) offered the best catalytic performance with a benzyl alcohol conversion of 13.6% under the optimized reaction condition (entry 5). As references samples, other carbon materials, such as ND (entry 2), 1500OLC (treated at 1500 °C, entry 6), 1600OLC (treated at 1600 °C, entry 7), graphene (entry 8) and graphite oxide (entry 9) showed a lower conversion of benzyl alcohol (4.9%~11.4%) and selectivity for benzaldehyde under the same reaction conditions. The decomposition efficiency of TBHP over 1300BND is apparently higher than that of the listed carbon materials, suggesting that the surface structure of 1300BND possesses a good activation capability for TBHP. It should be noted that the conversion of benzyl alcohol can be further improved to 62.3% along with a decent selectivity by prolonging the reaction time (entry 10).

The effect of solvent to catalytic performance was also investigated. The results in Table S1, entries 3-9 indicate that there is no direct relationship between the catalytic activity and the polarity value of the solvents. Moreover, 1300BND also displays an appreciable conversion of benzyl alcohol (13.4%, Table 1, entry 11) and selectivity of benzaldehyde (>99%) under solvent-free condition, which is comparable to commercial 5 wt% Pt/C and 5 wt% Ru/C (Table 1, entries 12, 14) catalysts, also in the absence of solvent, but being much better than the reported 5 wt% Pt/C, 5 wt% Ru/C and other noble-metal supported catalysts (Table 1, entries 13, 15-19) under similar reaction conditions.<sup>22,32-34</sup> In the previous studies, the trace amount of metal impurities (e.g., Fe<50 ppm, Cr< 10 ppm) has been found in 1300BND by an inductively coupled plasma optical emission spectrometer. Here, in order to exclude the roles of metal impurities, 0.1% Fe-, Cr-containing 1300BND samples were prepared by an annealing approach. The results indicate that metal-containing 1300BND catalysts cannot improve the catalytic performance in the selective oxidation of benzyl alcohol (Table 1, entries 13, 20-21).

**Table 2.** Selective oxidation of various substituted alcohols over 1300BND catalyst.<sup>[a]</sup>

Entry	Substrate	Product	t (h)	Con. (%)	Sel. (%)
1			12	43.3	98.2
2 <sup>[b]</sup>			6	30.2	>99
3 <sup>[b]</sup>			6	20.7	93.1
4			12	23.7	92.6
5 <sup>[b]</sup>			10	21.6	89.5
6 <sup>[b]</sup>			8	18.3	93.5
7			8 40	17.1 72.4	81.8 80.1
8 <sup>[b]</sup>			10	13.5	~70 <sup>[e]</sup> ~66 <sup>[f]</sup>
9 <sup>[b]</sup>			8	22.7	97.2
10 <sup>[b]</sup>			8	17.5	94.7
11 <sup>[c]</sup>			8	19.1	98.5
12 <sup>[c]</sup>			12	15.8	>99
13 <sup>[d]</sup>			12	12.2	90.9
14 <sup>[c]</sup>			12	10.9	91.3
15 <sup>[c]</sup>			20	17.2	88.1
16 <sup>[c]</sup>			12	12.8	84.3
17 <sup>[d]</sup>			20	14.9	89.2

18 <sup>[c]</sup>			20	10.8	87.1
19 <sup>[d]</sup>			12	14.9	77.2
20			20	21.1 34.2 <sup>[g]</sup>	73.2 62.1 <sup>[g]</sup>
21			20	21.7 37.4 <sup>[h]</sup>	79.0 60.2 <sup>[h]</sup>

[a] Reaction condition: 10 mg catalyst, 2.0 mmol substrate, 2.0 mmol TBHP, solvent-free, 70 °C. [b] 5 mL TFT as solvent. [c] 5 mL TFT as solvent, 1.0 mmol substrate, 2.0 mmol TBHP. [d] 1.0 mmol substrate, 2.0 mmol TBHP, solvent-free. [e] Ref 35, 1.5 mmol substrate, 20 mg Mn<sub>2</sub>O<sub>4</sub>/porous organic polymers as catalyst, 10 mL CH<sub>3</sub>CN, 3 mmol TBHP, 80 °C, 8 h. [f] Ref 36, n(substrate):(cat) =50, n(TBHP):(substrate)=2, [Fe(bipy)<sub>3</sub>](OTf)<sub>2</sub> as catalyst, 25 °C, 24 h. [g] The reaction conditions are the same as stated in footnote a, except the catalyst used is 5 wt% Pt/C. [h] The reaction conditions are the same as stated in footnote a, except the catalyst is 5 wt% Ru/C.

Since the preliminary results for the selective oxidation of benzyl alcohol seems positive over 1300BND catalyst, the substrate scope of the oxidation reaction was further examined. In Table 2, the results show that 1300BND catalyst was effective for the alcohols with mono-, di-, multi-substituted, heterocyclic, linear-chain and unsaturated structures. There were reasonable conversion and selectivity outputs under the optimized reaction conditions for all of the primary alcohols studied, especially under solvent-free conditions. For example, the selective oxidation of para-substituted alcohols, including 4-methylbenzyl alcohol, 4-nitrobenzyl alcohol, 4-methoxybenzyl alcohol, 4-fluorobenzyl alcohol, 4-chlorobenzyl alcohol and 4-biphenylmethanol resulted in a substrate conversion of 17.5%~43.3%, accompanying by excellent selectivities (>89.5%) towards the desired products (Table 2, entries 1-5, 10). Moreover, reasonable catalytic activity for the oxidation of unsaturated alcohols, such as cinnamic alcohol and 4-cyanobenzyl alcohol, could be achieved (Table 2, entries 7-8). It is worth to note that the selectivity for cinnamyl aldehyde (81.8%) is higher than that of the reported transition-metal catalysts.<sup>35-36</sup> Moreover, the conversion of cinnamic alcohol can be further improved to 72.4% along with a decent selectivity by prolonging the reaction time (entry 7). Recently, the production of aldehydes relies on the use of carbocatalysts and metal-based catalysts that possess selective oxidation of alcohol groups in the presence of some easily oxidizable functionalities. Here, 1300BND catalyst is also competent in the oxidation of di- and tri- substituted alcohols (Table 2, entries 12-17), those include methyl (e.g., 3, 4-dimethylbenzyl alcohol)-, methoxy (e.g., 3, 4-dimethoxybenzyl alcohol, 2, 3, 4-trimethoxybenzyl alcohol)-, halogenated (e.g., 3-fluoro-4-methoxybenzyl alcohol, 4-fluoro-2-methylbenzyl alcohol)-, nitro-groups (e.g., 2-chloro-5-nitrobenzyl alcohol), even in heterocycle-substituted alcohols (Table 2, entries 6, 18-19, e.g., 3-pyridinecarboxaldehyde, 1-benzothiophen-2-ylmethanol, cyclohexylmethanol) under solvent or solvent-free condition. The conversion of the alcohols and the selectivity for the corresponding aldehydes reached 10.9%~18.3% and 77.2~99%, respectively. In addition, the oxidation of linear-chain alcohols (e.g., 5-hexen-1-ol, 1-hexanol) could achieve a

comparable selectivity to 5 wt% Pt/C and 5 wt% Ru/C (Table 2, entries 20-21) under solvent-free condition. It is clear that 1300BND as an efficient carbocatalyst could deliver an excellent performance in the selective oxidation of various alcohols to their corresponding aldehydes.

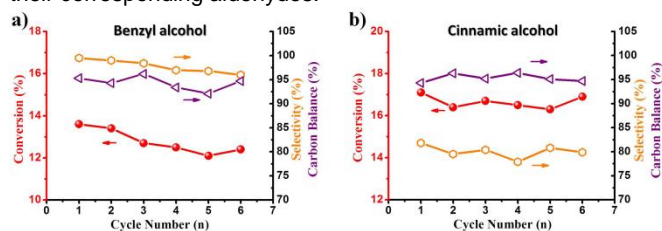


**Figure 1.** Catalytic stability of 1300BND for the selective oxidation of a) benzyl alcohol under solvent condition and b) cinnamic alcohol under solvent-free condition, 8 h.

The catalytic stability of catalyst was studied as well. The conversions of representative benzyl alcohol and cinnamic alcohol over 1300BND are 12.4% and 16.9 % along with the corresponding aldehydes selectivity of 96.5% and 80.0%, respectively, even after six successive runs (Figure 1). These indicated that 1300BND exhibits good stability upon recycling. The carbon balances of each run were verified by taking into account the unreacted alcohols, the produced aldehydes, the unreacted oxidant and the main product from the decomposition of oxidant. The carbon balance was calculated to be ~ 95 % of benzyl and cinnamic alcohol reactions and the small loss may be ascribed to the production of open-ring aromatic compounds and carbon oxides deriving from over-oxidation of the aldehydes.

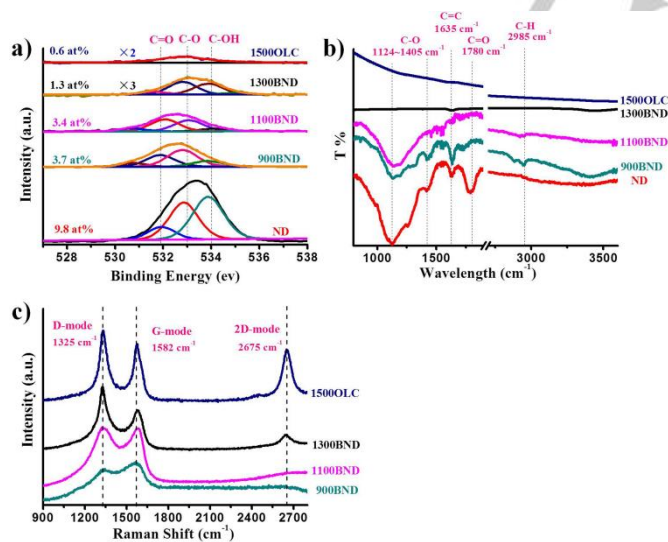


**Figure 2.** (a) O 1s XPS spectra, (b) FTIR spectra and (c) Raman spectra of ND, BND and OLC samples. The O1s XPS spectra are divided by fitting the peak maximum within  $\pm 0.1$  eV and applying a full width at half-maximum (FWHM) of 1.4–1.6 eV. The value of the mixed Gaussian-Lorentzian is maintained at 40%.

Previous studies in metal-free catalysis have shown that the surface functional groups (e.g., carbonyl groups) and defects in nanocarbons play important roles in promoting catalytic reactions and thus are considered to be possible active sites for the particular reactions.<sup>37-40</sup> In order to study the origin of the catalytic performance, the surface properties of the catalysts were characterized by XPS, FTIR and Raman spectroscopy. Figure 2a is the XPS O 1s spectra of ND, BND and OLC materials, deconvoluted into three peaks corresponding to unsaturated carbonyl group (C=O, ~531.8 eV), carbon-oxygen ester-like single group or anhydride (C-O, ~532.9 eV) and phenolic group (C-OH, ~534.0 eV). The total concentration of oxygen decreases from 9.8 at% of ND to 0.6 at% of 1500OLC. There is only little phenolic group found in 1500OLC. The FTIR spectra confirm the results from XPS and reveal the same surface groups over ND, such as C-O (1124–1405  $\text{cm}^{-1}$ ), C=C (~1635  $\text{cm}^{-1}$ ), C=O (~1780  $\text{cm}^{-1}$ ) and C-H (~2985  $\text{cm}^{-1}$ ), as shown in Figure 2b. The intensity weakening of various carbon-related signal peaks over BND should be attributed to its the decrease of the content of the surface groups. No obvious peaks could be observed for 1500OLC. On the aspect of structure-activity relationship, it may be found that 1300BND, which exhibited the best catalytic activity, has a low oxygen content (only 1.3 at%). On the contrary, ND, which carries the highest concentration of surface oxygen, showed a poor conversion of substrate (Table 1, entry 2). The correlations within different kinds of oxygen species (C=O, C-O and C-OH) and catalytic performance were studied in detailed in Figure S2, and the results suggest that the content of surface oxygen species was not proportional to the mass-normalized activity. In other words, there may be no direct relationship between surface oxygen groups and catalytic performance. To verify this hypothesis, 1600OLC, which has a similar content of oxygen species (0.54 at%, see Figure S3a) to 1500OLC (0.61 at%), was used as a reference, and the corresponding catalytic activity reflected that the 1600OLC exhibited a lower conversion of substrate than that of 1500OLC (Table 1, entries 6-7). All the results suggest that the surface oxygen groups may be inconsequential to the selective oxidation of alcohols.

Raman spectroscopy is a powerful tool to study surface defect of the samples. The intensity of the D-band was allowed as probes for the formation of a disordered graphitic lattice structure (graphene layer edges).<sup>41</sup> As shown in Figure 2c, the D-bands (~1325  $\text{cm}^{-1}$ ) of BND and OLC significantly enhance with increasing the synthesis temperature from 900 °C to 1500 °C, which are attributed to the phase transformation of  $\text{sp}^2/\text{sp}^3$  hybridized BND to  $\text{sp}^2$  hybridized OLC.<sup>42</sup> Besides, comparing with 900 BND and 1100 BND, the appearance of 2D-band (~2675  $\text{cm}^{-1}$ ) over 1300BND and 1500OLC suggests that their surface carbon structures should consist of stacked graphene layers. It can be found that 1300BND, with a better catalytic activity, shows a stronger D-band than that of 900 BND and 1100 BND. In this case, it seems that the concentration of graphitic edges can affect the catalytic performance. The value of the ID/IG ratio was further used as a quantitative measure of the structural defects. Compared with 1500OLC ( $I_D/I_G=1.12$ , calculated by the intensity ratio), 1300BND ( $I_D/I_G=1.31$ ) also

exhibited better catalytic activity. It is worth noting that when 1600OLC, having a smaller  $I_D/I_G$  value (1.05, Figure S3b), was introduced into this reaction, the corresponding conversion of benzyl alcohol (9.3%, Table 1, entry 7) is lower than that of 1500OLC (11.4%, Table 1, entry 6). The comparative results of 1300BND, 1500OLC and 1600OLC provided an evidence for the important roles of structural defects in the selective oxidation of benzyl alcohol.

**Table 3.** Catalytic performance of benzyl alcohol over various model molecule catalysts.<sup>[a]</sup>

Entry	Model catalyst	Mimicked structure	Con. (%)	Sel. (%)	Yield (%)	Decomposition efficiency (%) of TBHP
1 <sup>[b]</sup>	Blank	----	2.5	90.3	2.3	1.8
2		phenol	2.9	84.7	2.5	2.6
3		quinones	3.9	84.5	3.3	4.0
4		armchair	3.5	83.6	2.9	2.4
5		armchair	3.8	86.9	3.3	2.9
6		zigzag	3.4	91.4	3.1	6.9
7		zigzag	4.8	89.8	4.3	17.7
8		zigzag	6.3	92.0	5.9	28.2
9		zigzag	8.6	94.5	8.1	41.4
10		zigzag ether	4.1	81.1	3.3	3.7
11		zigzag quinones	5.1	89.2	4.5	18.8

[a] Reaction conditions: 1 mmol model catalyst, 2 mmol substrate, 2 mmol TBHP, 5 mL TFT, T = 70 °C, 4 h.

[b] Conducted in the absence of catalyst. Desired product: benzaldehyde.

Defects are abundant in carbon materials and have been considered as an essential constituent of carbon network structure with abundant chemical information. Although possible roles of defects in metal-free catalysis have been studied by using Raman measurements and theoretical calculations over the past few years,<sup>19, 40, 43-44</sup> there is still a lack of an effective method to identify the type of defects and to give an accurate description of the amounts of each type, not even to mention the total number of defects per unit area. As such, revealing the structure-activity relationship of defects in a reaction process is still a great challenge. As compared to nanocarbon materials, aromatic organic molecules (e.g., anthracene, phenanthrene) have a similar carbon network structure and a tunable electronic conjugated  $\pi$  system (by extending the carbon unit) that can be

directly used to simulate the structures of carbon catalysts and to identify specific active sites, such as zigzag and armchair configurations. Here we use several small molecules with defined structures as model catalysts to further investigate possible active defect sites and the corresponding activation capacities for oxidant. As mentioned, the roles of oxygen groups in the reaction have been excluded based on XPS and IR techniques. As shown in Table 3, model catalysts with C=O, C-OH and C-O groups (entries 2-3 and 10) do not exhibit a prominent catalytic activity as compared to the blank experiment. This result well supported the non-participation of the surface oxygen groups for selective oxidation of benzyl alcohol. We also applied a few model catalysts with specific armchair and zigzag configurations to identify the types of active defect sites. Two model catalysts with an armchair structure did not exhibit an improved catalytic activity (Table 3, entries 4-5); the selectivity towards benzaldehyde was even lower than that of the blank experiment. In contrast, the conversion of benzyl alcohol (3.4%~8.1%) and the selectivity towards benzaldehyde (89.8%~94.5%) were remarkably improved with increasing of the zigzag unit of the model catalysts (Table 3, entries 6-9). All these facts indicate that zigzag configuration should have an important role in facilitating the selective oxidation of benzyl alcohol. In addition, there was no conspicuous synergistic effect between the zigzag and oxygen species (C-O, C=O) since the observed yields were only 3.3 % and 4.5 % on xanthenes and pentacenequinone catalysts (entries 10-11), respectively. The decomposition efficiency of TBHP over different model catalysts was evaluated in detail. As displayed in Table 3, the model catalysts with zigzag configuration exhibited better decomposition efficiencies of TBHP (6.9~41.4%) than other catalysts, which are directly proportional to their catalytic performances (entries 6-9). The same relationship can be found in used nanocarbon catalysts (Table 1, entries 2-9). These observations provided evidence to the fact that the zigzag configuration has an excellent activation capacity for TBHP and thus might be active site in the selective oxidation of alcohols.

Redox potential is an important descriptor in electrochemistry that reflects the extra potential energy required to initiate or activate reactant species, i.e., the oxidant or substrate. Catalytic systems with a smaller onset potential is more likely to proceed under conditions with less energy input. Cyclic voltammetry (CV) was firstly performed to measure the ability to activate the substrate (BA) and oxidant (TBHP) by the catalyst (Cat, anthracene was used as a representative catalyst) under an ex-situ reaction condition. Figure 3a shows the voltammograms of the system components and the oxidation onset potentials are determined. It is clear that the oxidation onset potentials for the BA and TBHP are above 1.3 V (vs. Ag/Ag+). When TBHP and BA were together introduced to the system, the slight enhancement in the current and reduction in onset potential are indications of their interaction during the electrochemical oxidation. Such interaction adequately explains for the 2.5% BA conversion and the TBHP decomposition efficiency of 1.8% in a blank experiment. Interestingly, as the catalyst was added,

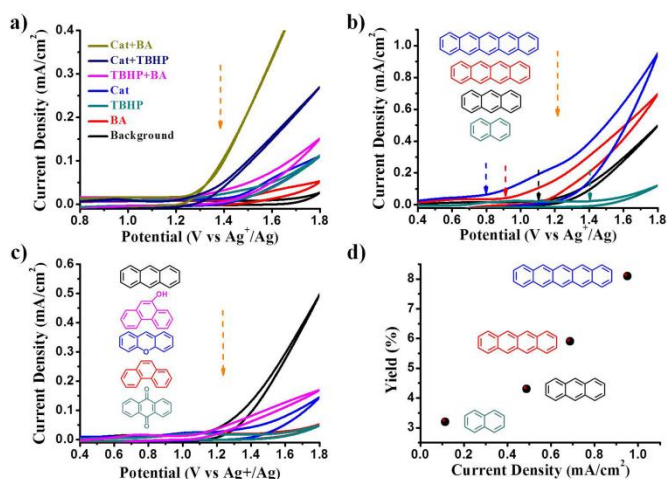


**Figure 3.** Ex-situ cyclic voltammograms (100 mV/s) of benzyl alcohol oxidation in 0.045 M TBAPF<sub>6</sub>/TFT electrolyte under (a) systems with different components, (b) systems using model catalysts with different zigzag structure and (c) systems using model catalysts with varying oxygen species and armchair structures. (d) The dependence of apparent current density (at 1.8 V) on the catalytic activity over different model catalysts with zigzag structure for the selective oxidation of benzyl alcohol; Cat used in (a) is anthracene and BA denotes benzyl alcohol. The test conditions: 0.02 mmol model catalysts (Cat), 2 mmol benzyl alcohol (BA), 2 mmol TBHP, 5 mL TBAPF<sub>6</sub>/TFT electrolyte, 25 °C.

the onset potential decreased from c.a. 1.45 V (BA) to 1.25 V (Cat+BA) for the BA system, while that for TBHP system decreased from c.a. 1.35 V (TBHP) to 1.3 V (Cat+TBHP). At the same time, the corresponding current densities for both systems showed significant improvement with the catalyst as compared to that when without. The higher oxidation current and the lower oxidation onset potential of Cat+BA system to BA imply that catalyst may activate the hydrogen atom of -CH<sub>2</sub>OH group of BA. Similarly, the obvious differences of Cat+TBHP system to TBHP on current and oxidation potential suggest that edge structure could facilitate the decomposition of TBHP into tBuOO•, tBuO• and •OH radicals under reaction conditions. It is worth noting that the current enhancement in Cat+BA/BA is more prominent to that in Cat+TBHP/TBHP. This suggests that BA is more readily activated on the catalyst and thus being more vulnerable to oxidation. The enhancements may be ascribed to the edge structures of the catalyst and the interaction with the reactants. These observations demonstrate that anthracene as a model catalyst can effectively activate substrate and oxidant in the selective oxidation of benzyl alcohol. This is consistent with the experimental results of the improved decomposition efficiency of TBHP and the catalytic activity over anthracene. It should be noted that other model catalysts with elongated zigzag edges exhibited further enhancement in terms of the reduced onset potential and increased Faradaic current density (Figure 3b). For instance, the onset potential for the system with pentacene is close to 0.8 V, which is far less than that of anthracene (1.1 V).

Besides, the corresponding onset oxidation potentials/currents for model catalysts with different oxygen

species and armchair configuration are higher/lower than that of anthracene (Figure 3c), respectively. This can be attributed to (1) zigzag edge may be more reactive than the armchair edge due to its unique electronic structure and unpaired electrons;<sup>45-46</sup> (2) the incorporation of oxygen to edge structure may deteriorate the  $\pi$ -conjugated system of graphitic lattice and thus weaken the activation ability for the oxidant. The electrochemical results further excluded the roles of oxygen species and armchair edge structure in the catalytic reaction. Moreover, there is a directly proportional relationship between the yield and the oxidation current density (Figure 3d), suggesting a good correlation between electrochemical and thermal reactions. It is therefore reasonable to expect that the zigzag edges are the active structure in the selective oxidation of benzyl alcohol, thanks to the excellent decomposition efficiency for oxidant and the activation ability for substrate thereby lower the onset oxidation potential and enhance the higher oxidation current relative to other species.

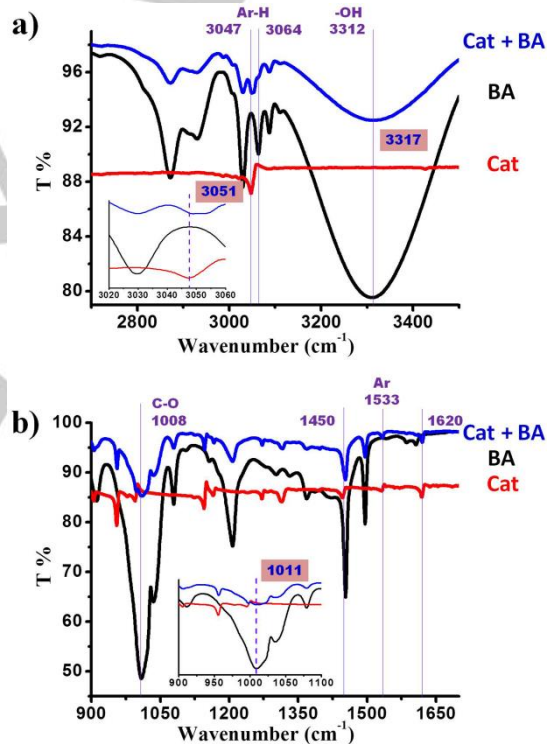


**Figure 4.** Ex-situ attenuated total reflectance (ATR) spectra of anthracene for the activation process of benzyl alcohol. The spectra were normalized by subtracting the signals of TFT. The test conditions: 0.02 mmol model catalyst (Cat, red line), 2 mmol benzyl alcohol (BA, black line), 5 mL TFT, 70 °C, 4 h.

As mentioned above, zigzag configuration may activate the hydrogen atom of -CH<sub>2</sub>OH group of BA. Here, we performed ex-situ ATR experiments to monitor the chemical state at the working surface. As shown in Figure 4a, compared with pure BA, the introduction of Cat does not change the bands position of -CH<sub>2</sub> stretching vibration of -CH<sub>2</sub>OH group (2800~2900 cm<sup>-1</sup>).<sup>47</sup>

On the contrary, the blue-shift (from 3312  $\text{cm}^{-1}$  of BA to 3317  $\text{cm}^{-1}$  of Cat+BA) of -OH band indicates that Cat can weaken the interaction between O and H atoms, that is, -OH may be activated. The similar blue-shift (from 3047  $\text{cm}^{-1}$  of pure Cat to 3051  $\text{cm}^{-1}$  of Cat+BA, see the inset of Figure 4a) of -CH stretch of benzene ring (Ar-H) shows that there is a weak interaction between -OH and Cat. As displayed in Figure 4b, the peaks located at about 1008  $\text{cm}^{-1}$  and 1450, 1533, 1620  $\text{cm}^{-1}$  are assigned to the stretching vibration band of C-O and the C=C vibration bands of benzene ring, respectively. Compared with pure BA and pure Cat, both the blue-shifts of C-O peak (shifts from 1008  $\text{cm}^{-1}$  to 1011  $\text{cm}^{-1}$  of Cat+BA, see the inset of Figure 4b) and C=C peak (at 1450  $\text{cm}^{-1}$ ) of Cat+BA suggest that the weak interaction may be  $\text{Ar}\cdots\text{H}-\text{O}-\text{CH}_2-\text{R}$ , that is, Cat can activate the hydrogen atom of -OH group rather than -CH<sub>2</sub> group.

The ·OH radicals derived from decomposition of TBHP over zigzag edge defect may capture the activated hydrogen atom on the -OH of the -CH<sub>2</sub>OH, along with the release of H<sub>2</sub>O and the formation of a -CH<sub>2</sub>O group (Figure 5). On the other hand, it has been reported that the tBuOO·, tBuO· radicals from the decomposition of TBHP could extract an hydrogen atom derived from the C-H bond of the -CH<sub>2</sub>O group,<sup>48-49</sup> and subsequently leading to the formation of aldehydes (-CHO group), tert butyl alcohol (tBuOH) and tBuOOH. The produced tBuOOH can be reused in the reaction. The detailed process can be found in Figure 5.

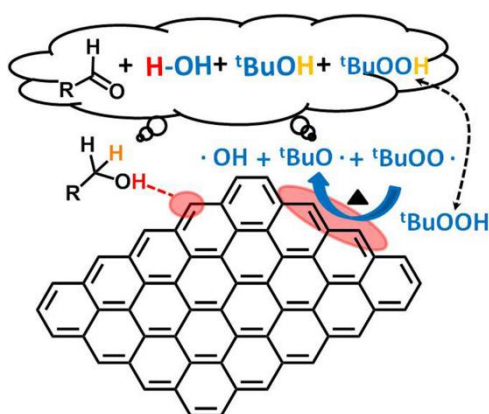


**Figure 5.** The possible mechanism diagram of catalytic reaction for selective oxidation of alcohols on BND (graphite planes with zigzag configuration is used as an ideal catalyst surface).

## Conclusions

In summary, an effective catalytic reaction pathway for the selective oxidation of alcohols with various functionalities and structures has been investigated with bucky nanodiamond (BND) as catalyst. The excellent selectivity for desired products (>73.2%) can be achieved at a mild reaction condition, even in a solvent-free condition. It was found that the edge defects with a zigzag configuration play an important role in the catalytic process, based on the excellent decomposition capability for TBHP and the effective activation for substrate, as

elucidated by the model catalysts, the ex-situ electrochemical and the ex-situ attenuated total reflectance studies. The best oxidation onset potential of model catalysts with a zigzag structure is as low as 0.8 V (i.e., a rather low extra potential for activation reaction). It was revealed that the surface oxygen groups do not carry a key role in the reaction. This work is anticipated to form a basis for the insight into the roles of defects and oxygen species in carbon materials in liquid-phase catalytic oxidation reactions.

## Experimental Section

### Experimental Materials

Benzyl alcohol (99%+), anthraquinone (99%), phenanthraquinone (99%), trifluorotoluene (TFT, 99%), tert-butyl hydroperoxide (TBHP, ~65 wt% in water), phenanthrene (99%), anthrone (97%), anthracene (99%), dimethyl carbonate (DMC, 99%) and 5% Pt/C were purchased from Alfa. Picene (purified by sublimation, 99.5%), xanthene (98%), naphthacene (97%) and fluorene (97%) were supplied by TCI. Pentacene (98%), 6,13-pentacenequinone (99%), tetrabutylammonium hexafluorophosphate and 5% Ru/C were supplied by Acros. 9-phenanthrenol was obtained from Sigma-Aldrich. Graphite was provided by ACHESON Co. Ltd. Acetonitrile tetrahydrofuran (THF), dimethyl formamide (DMF), dioxane, hexane and dichloromethane (DCM) were all from Sinopharm Chemical Reagent Co., Ltd. All reagents were used without further purification. Purified ultra-dispersed nanodiamond (ND) was bought from Beijing Grish Hitech Co. (China), produced by detonation and purified by acid washing; the average particle size is ~5 nm. The noncombustible contaminations were tested by an inductively coupled plasma optical emission spectrometer (ICP-OES) and included Fe < 50 ppm, Cr < 10 ppm, Al < 50 ppm, Cu < 10 ppm, Mg < 10 ppm, Ti < 10 ppm, and Ca < 50 ppm. Graphene (99%) was supplied by Tanmei Ltd, Co. (China).

### Samples preparation

900BND, 1100BND and 1300BND with graphite-like shell structures were produced by annealing purified ND at 900, 1100 and 1300 °C for 4 h in argon atmosphere, respectively. Similarly, 1500OLC and 1600OLC can be obtained by annealing ND at 1500 and 1600 °C for 30 min in an Ar atmosphere, respectively.

### Characterization

High-resolution transmission electron microscopy (HRTEM) was conducted on a FEI Tecnai G2 F20 microscope. The X-ray photoelectron spectroscopy (XPS) was performed on an ESCALAB 250 XPS system with a monochromatized Al K-alpha X-ray source. N<sub>2</sub> adsorption-desorption was carried out on the Micromeritics ASAP2020 setup and analyzed applying Brunauer-Emmett-Teller (BET) theory. Raman spectra of samples on SiO<sub>2</sub>/Si were collected with a LabRam HR800 spectrometer and a He/Ne laser at 532 nm (50xobjective) was selected as the excitation source. Moreover, the laser power and exposure time were maintained low to avoid local damage of samples by the heating. All electrochemical measurements were operated by Epsilon Electrochemical workstation (PAR2273) at 25 °C. The measurements were performed with a three-electrode system using polished glassy carbon electrodes as both the counter electrode and working electrode, and a non-aqueous Ag/Ag<sup>+</sup> reference electrode stabilized in a 0.045 M tetrabutylammonium hexafluorophosphate (TBAPF<sub>6</sub>)/trifluorotoluene

(TFT). The whole electrochemical measurement system was almost similar to the alcohol oxidation reaction conditions except reaction temperature. TBAPF<sub>6</sub> was used as a conductive additive. Therefore, the electrochemical method was an ex-situ measurement technique. FTIR and attenuated total reflectance (ATR) were collected at a resolution of 4 cm<sup>-1</sup> on Nicolet iS50 at room temperature (25 °C) and reaction temperature (70 °C), respectively.

The alcohol oxidation reactions were operated in a 48 ml pressure bottle containing certain amounts of catalyst, substrates and oxidant. A given amount of ethylbenzene was added as an internal standard in the reaction solution after reaction for product analysis. The reaction solution was sampled periodically and analyzed using gas chromatography with a HP-5 column (Agilent 7890A). Conversion, yield, and selectivity for the oxidation of alcohols to target products were defined as follows:

$$\text{Conversion (\%)} = [(C_0 - C_r) / C_0] \times 100$$

$$\text{Yield (\%)} = C_p / C_0 \times 100$$

$$\text{Selectivity (\%)} = [C_p / (C_0 - C_r)] \times 100$$

where C<sub>0</sub> is the initial concentration of alcohol, and C<sub>r</sub> and C<sub>p</sub> are the concentration of reactants and products, respectively, at a certain time after the reaction. The concentration of reactants and products can be measured by an internal standard method (based on integral area method). The carbon balance based on the observed products can be calculated as:

$$\text{Carbon balance (\%)} = [(C_{\text{aldehydes}} + C_{\text{tert-butyl alcohol}} + C_{\text{residue, alcohols}} + C_{\text{residue, oxidant}}) / (C_0, \text{alcohols} + C_0, \text{oxidant})] \times 100$$

where C<sub>aldehydes</sub>, C<sub>residue, alcohols</sub>, C<sub>tert-butyl alcohol</sub>, C<sub>residue, oxidant</sub> are the concentrations of aldehydes, unreacted alcohols, tert-butyl alcohol (the main product derives from the decomposition of TBHP during the reaction) and unreacted TBHP, respectively.

## Acknowledgements ((optional))

The authors acknowledge the financial support from "Strategic Priority Research Program" of the Chinese Academy of Sciences, Grant No. XDA09030103.

**Keywords:** nanodiamond • selective oxidation • electrochemical • carbocatalysis • redox potential

- [1] G.-J. T. Brink, I. W. C. E. Arends, R. A. Sheldon, *Science*, **2000**, *287*, 1636-1639.
- [2] R. Liu, X. Liang, C. Dong, X. Hu, *J. Am. Chem. Soc.*, **2004**, *126*, 4112-4113.
- [3] H. Wang, W. Fan, Y. He, J. Wang, J. N. Kondo, T. Tatsumi, *J. Catal.*, **2013**, *299*, 10-19.
- [4] T. Mallat, Baiker, *A. Chem. Rev.*, **2004**, *104*, 3037-3058.
- [5] D. I. Enache, J. K. Edwards, P. Landon, B. Solsona-Espriu, A. F. Carley, A. A. Herzing, M. Watanabe, C. J. Kiely, D. W. Knight, G. J. Hutchings, *Science*, **2006**, *311*, 362-365.
- [6] B.-Z. Zhan, M. A. White, T.-K. Sham, J. A. Pincock, R. J. Doucet, K. V. Ramana Rao, K. N. Robertson, T. S. Cameron, *J. Am. Chem. Soc.*, **2003**, *125*, 2195-2199.

- [7] S. Yin, J. Lia, H. Zhang, *Green Chem.*, **2016**, *18*, 5900-5914.
- [8] T. Wang, X. Yuan, S. Li, L. Zeng, J. Gong, *Nanoscale*, **2015**, *7*, 7593-7602.
- [9] P. Weerachawanasak, J. Hutchings, G. J. K. Edwards, S. A. Kondrat, P. J. Miedziak, P. Prasertham, J. Panpranot, *Catal. Today*, **2015**, *250*, 218-225.
- [10] A. Abad, P. Concepcion, A. Corma, H. Garcia, *Angew. Chem. Int. Ed.*, **2005**, *44*, 4066-4069.
- [11] H. Tsunoyama, H. Sakurai, Y. Negishi, T. Tsukuda, *J. Am. Chem. Soc.*, **2005**, *127*, 9374-9375.
- [12] N. Dimitratos, J. A. Lopez-Sanchez, D. Morgan, A. Carley, L. Prati, G. J. Hutchings, *Catal. Today*, **2007**, *122*, 317-324.
- [13] N. Dimitratos, J. A. Lopez-Sanchez, D. Morgan, A. Carley, R. Tiruvalam, C. J. Kiely, D. Bethell, G. J. Hutchings, *Phys. Chem. Chem. Phys.*, **2009**, *11*, 5142-5153.
- [14] A. Abad, C. Almela, A. Corma, H. Garcia, *Tetrahedron*, **2006**, *62*, 6666-6672.
- [15] A. Villa, N. Janjic, P. Spontoni, D. Wang, D. S. Su, L. Prati, *Appl. Catal. A: Gen.*, **2009**, *364*, 221-228.
- [16] W. Li, Y. Gao, W. Chen, P. Tang, W. Li, Z. Shi, D. Su, J. Wang, D. Ma, *ACS Catal.*, **2014**, *4*, 1261-1266.
- [17] Y. Gao, G. Hu, J. Zhong, Z. Shi, Y. Zhu, D. Su, J. Wang, X. Bao, D. Ma, *Angew. Chem. Int. Ed.*, **2013**, *52*, 2109-2113.
- [18] Y. Lin, X. Pan, W. Qi, B. Zhang, D. S. Su, *J. Mater. Chem. A*, **2014**, *2*, 12475-12483.
- [19] D. S. Su, S. Perathoner, G. Centi, *Chem. Rev.*, **2013**, *113*, 5782-5816.
- [20] J. Luo, F. Peng, H. Yu, H. Wang, *Chem. Eng. J.*, **2012**, *204*, 98-106.
- [21] Y. Kuang, N. M. Islam, Y. Nabaie, T. Hayakawa, M.-a. Kakimoto, *Angew. Chem.*, **2010**, *122*, 446-450.
- [22] Y. Lin, D. Su, *ACS Nano*, **2014**, *8*, 7823-7833.
- [23] Y. Meng, D. Voiry, A. Goswami, X. Zou, X. Huang, M. Chhowalla, Z. Liu, T. Asefa, *J. Am. Chem. Soc.*, **2014**, *136*, 13554-13557.
- [24] A. Gharib1, L. V. Fard, N. N. Pesyan, M. Roshani, *Chemistry*, **2015**, *1*, 151-158.
- [25] M. A. Patel, F. Luo, M. R. Khoshi, E. Rabie, Q. Zhang, Carol R. Flach, R. Mendelsohn, E. Garfunkel, M. Szostak, H. He, *ACS Nano*, **2016**, *10*, 2305-2315.
- [26] H. Watanabe, S. Asano, S.-i. Fujita, H. Yoshida, M. Arai, *ACS Catal.*, **2015**, *5*, 2886-2894.
- [27] T. Petit, J. C. Arnault, H. A. Girard, M. Sennour, T. Y. Kang, C. L. Cheng, P. Bergonzo, *Nanoscale*, **2012**, *4*, 6792-6799.
- [28] X. Sun, R. Wang, B. Zhang, R. Huang, X. Huang, D. S. Su, T. Chen, C. Miao, W. Yang, *ChemCatChem*, **2014**, *6*, 2270-2275.
- [29] R. Wang, X. Sun, B. Zhang, X. Sun, D. S. Su, *Chem. Eur. J.*, **2014**, *20*, 6324-6331.
- [30] V. L. Kuznetsov, A. L. Chuvilin, Y. V. Butenko, I. Y. Mal'kov, V. M. Titov, *Chem. Phys. Lett.*, **1994**, *222*, 343-348.
- [31] Z. Qiao, J. Li, N. Zhao, C. Shi, Philip. Nash, *Scripta Mater.*, **2006**, *54*, 225-229.
- [32] V. Peneau, Q. He, G. Shaw, S. A. Kondrat, T. E. Davies, P. Miedziak, M. Forde, N. Dimitratos, C. J. Kiely, G. J. Hutchings, *Phys. Chem. Chem. Phys.*, **2013**, *15*, 10636-10644.
- [33] V. R. Choudhary, D. K. Dumbre, *Ind. Eng. Chem. Res.*, **2009**, *48*, 9471-9478.
- [34] V. R. Choudhary, D. K. Dumbre, *Appl. Catal. A: Gen.*, **2010**, *375*, 252-257.
- [35] K. Dhanalaxmi, R. Singuru, S. K. Kundu, B. M. Reddy, A. Bhaumik, John. Mondal, *RSC Adv.*, **2016**, *6*, 36728-36735.
- [36] J. E. Chàveza, C. Crottib, E. Zangrandoa, E. Farnettia, *J. Mol. Catal. A: Chem.*, **2016**, *421*, 189-195.
- [37] S. Wu, G. Weng, J. Wang, J. Rong, B. Zong, D. S. Su, *Catal. Sci. Technol.*, **2014**, *4*, 4183-4187.
- [38] S. Wu, G. Weng, X. Liu, B. Zhong and D. S. Su, *ChemCatChem*, **2014**, *6*, 1558-1561.

- [39] G. Weng, S. Wu, B. Li, C. Dai, D. S. Su, *Angew. Chem. Int. Ed.*, **2015**, *54*, 4105-4109.
- [40] Y. Lin, B. Li, Z. Feng, Y. A. Kim, M. Endo, D. S. Su, *ACS Catal.*, **2015**, *5*, 5921-5926.
- [41] R. Huang, J. Xu, J. Wang, X. Sun, Wei. Qi, C. Liang, D. S. Su, *Carbon*, **2016**, *96*, 631-640.
- [42] M. Zeiger, N. Jackel, V. N. Mochalin, V. Presser, *J. Mater. Chem. A*, **2016**, *4*, 3172-3196.
- [43] S. Song, H. Yang, R. Rao, H. Liu, A. Zhang, *Catal. Commun.*, **2010**, *11*, 783-787.
- [44] G. L. Chai, Z. Hou, D.J. Shu T. Ikeda, K. Terakura, *J. Am. Chem. Soc.*, **2014**, *136*, 13629-13640.
- [45] J. H. Yang, G. Sun, Y. Gao, H. Zhao, P. Tang, J. Tan, A. H. Lu, D. Ma, *Energy Environ. Sci.*, **2013**, *6*, 793-798.
- [46] T. Enoki, Y. Kobayashi, K. I. Fukui, *Int. Rev. Phys. Chem.*, **2007**, *26*, 609-645.
- [47] M. Thomas, H. H. Richardson, *Vib. Spectrosc.*, **2000**, *24*, 137-146.
- [48] E. C. McLaughlin, H. Choi, K. Wang, G. Chiou, M. P. Doyle, *J. Org. Chem.*, **2008**, *74*, 730-738
- [49] S. J. Jeon, H. Li, P. J. Walsh, *J. Am. Chem. Soc.*, **2005**, *127*, 16416-16425.

Entry for the Table of Contents (Please choose one layout)

FULL PAPER



Yangming Lin,<sup>[a,b,c]</sup> Kuang-Hsu (Tim) Wu,<sup>[a]</sup> Linhui Yu,<sup>[d]</sup> Saskia Heumann,<sup>[c]</sup> and Dang Sheng Su<sup>[a, e]</sup>\*

Page No. – Page No.

**Efficient and Highly Selective Solvent-Free Oxidation of Primary Alcohols to Aldehydes Using Bucky Nanodiamond**

An effective catalytic reaction pathway for the selective oxidation of primary alcohols with various functionalities and structures has been developed with bucky nanodiamond as catalyst. The zigzag edges of  $sp^2$  carbon planes have been shown to play a crucial role in these reactions.

Accepted Manuscript